Available online at www.sciencedirect.com
SCIENCE DIRECT®
International Journal of Heat and Fluid Flow 24 (2003) 242–259
International Journal of HEAT AND FLUID FLOW
www.elsevier.com/locate/ijhff

The droplet number moments approach to spray modelling: The development of heat and mass transfer sub-models

J.C. Beck, A.P. Watkins *

Atomisation and Sprays Research Group, Mechanical, Aerospace and Manufacturing Engineering Department, UMIST, Manchester M60 1QD, UK

Received 6 December 2001; accepted 27 November 2002

Abstract

In the past most poly-disperse spray models have been based on either discretising the liquid flow field into groups of equally sized droplets, as in the discrete droplet model (DDM) in which parcels of drops are tracked in space in a Lagrangian framework, or by solving separate Eulerian conservation equations for a number of size ranges. Both of these approaches can result in very long computing times, although the DDM is generally regarded as being superior in this respect under most conditions of interest. Recently an alternative approach to the modelling of sprays has been developed by Beck [Ph.D. Thesis, UMIST, 2000] and Beck and Watkins [Proc. R. Soc. Lond. A, 2003]. In this approach the size information concerning the spray is obtained by solving conservation and transport equations for two moments of the drop number distribution, and their respective mean velocities, and obtaining two other moments from an assumed size distribution function. The sub-models required in this approach, for hydrodynamic phenomena in sprays, such as drop drag, break-up and collisions, have been presented elsewhere [Beck, Ph.D. Thesis, UMIST, 2000; Beck and Watkins, J. Comp. Phys., 2002]. The purpose of this paper is to present those sub-models relating to the mass and heat transfer processes in sprays. As part of this, an equation for the energy of the liquid phase is required. Standard gas phase equations, including a k–ε turbulence model, are also solved. All the equations are solved in a Eulerian framework using the finite-volume approach. The inter-phase heat and mass transfers are captured through the use of source terms, and all the source terms for these aspects of the spray model are derived in this paper in terms of the four moments of the droplet number distribution in order to find the net effect on the whole spray flow field. The model has been applied to a wide variety of different sprays, including high-pressure diesel sprays, wide-angle solid cone water sprays, hollow cone sprays and evaporating sprays [Beck, Ph.D. Thesis, UMIST, 2000]. The comparisons of the results with experimental data show that the model generally performs well. In this paper the evaporation effects are examined and compared with experimental data wherever possible. Again this aspect of the spray model is shown to be generally successful.

Keywords: Sprays; Modelling; Sub-models; Droplet number moments; Heat and mass transfer

1. Introduction

The majority of computational spray models employ the particle-source-in-cell method (Crowe et al., 1977) or the discrete droplet model (DDM), Ducowicz (1980). The DDM has been employed for a wide range of spray simulations, particularly fuel sprays in engines (Gosman and Johns, 1980; Reitz, 1987; Amsden et al., 1989; Watkins, 1989; Chen and Perreira, 1992). The DDM involves solving the equations of motion for a turbulent carrier gas in a Eulerian scheme, and integrating Lagrangian equations of motion for liquid droplets along true path lines. These two calculation schemes, and therefore the two phases, are then coupled through source terms in the transport equations. The major advantages of this over a purely Eulerian scheme are the ability to efficiently discretise the liquid phase into groups of identical droplets, and the fact that the equations for the dispersed liquid phase are more naturally written down in a Lagrangian manner. The disadvantage of the DDM is that it is dependent on predicting the chaotic motions of individual droplets in order to provide an overall picture of the spray. The

* Corresponding author. Tel.: +44-161-200-3706; fax: +44-161-200-3723.
E-mail address: paul.watkins@umist.ac.uk (A.P. Watkins).

0142-727X/03/$ - see front matter © 2003 Elsevier Science Inc. All rights reserved.
doi:10.1016/S0142-727X(02)00242-4

Nomenclature

b	impact parameter
B_M	mass transfer number
B_{Q_i}	source term due to break-up
C_{coll}	collisions parameter
c_p	specific heat capacity
C_μ, $C_{\varepsilon 1}$, $C_{\varepsilon 2}$, $C_{\varepsilon 3}$	turbulence parameters
D	diameter
E	total energy
f	vapour mass fraction
k	thermal conductivity
k	turbulent kinetic energy
L	latent heat of vaporisation
M	molecular weight
m	mass
N_{coll}	number of collisions
$n(r)$	number distribution
Nu	Nusselt number
P	pressure
P	probability
p_k	generation of turbulence kinetic energy
p	partial pressure
p_r	pressure ratio
Q	droplet moment
Q_0	total number
Q_1	sum of radii
Q_2	sum of squares of radii
Q_3	sum of cubes of radii
R	gas constant
Re	Reynolds number
R_0	universal gas constant
r	drop radius
S	source term
Sc	Schmidt number
Sh	Sherwood number
T	temperature
t	time
U	velocity
V	volume
$v(r)$	volume size distribution
We	Weber number
x	coordinate direction, fraction

Greeks

α_R	Rosin–Rammler exponent
β	spray cone angle
δ_{ij}	Kronecker delta
ε	turbulence kinetic energy dissipation rate
Γ	diffusivity
μ	dynamic viscosity
ν	kinematic viscosity
θ	void fraction
ρ	density
σ	surface tension, turbulent Prandtl number

Subscripts

a	air
b	bag break-up
cell	cell
coal	coalescence
coll	collision
E	energy
eff	effective
evap	evaporation
exp	expansion
f, v	vapour
g	gas
i	moment index
i, j	velocity component
in	input to liquid
k	turbulence kinetic energy
l	liquid
lam	laminar
m	mass
mix	mixture of gases
p, q	mean diameter parameters
R	Rosin–Rammler
rel	relative
s	droplet surface, stripping break-up
sep	separation
t	turbulent
ε	dissipation rate
32	Sauter mean radius

Superscripts

n	new time level
o	old time level

stochastic models employed in producing this chaotic motion require a large number of drop parcels to produce a smooth representation of the spray and are therefore computationally expensive, although generally recognised to be more efficient in this regard than the current alternatives.

The Eulerian treatment (Harlow and Amsden, 1975; Crowe, 1982) is inherently more efficient than its Lagrangian counterpart (Mostafa and Mongia, 1987) and multi-size Eulerian treatments have been employed by similar discretisation of the droplet size distribution and consideration of each size group as a completely

separate phase, (Mostafa and Elghobashi, 1985). However, this leads to a scheme involving many phases, if the size distributions in the spray are to be fully captured, and is thus computationally very expensive.

An alternative approach to the modelling of poly-disperse sprays has been suggested by Beck (2000). The liquid and the gas are both represented in the more efficient Eulerian formulation, and the full poly-disperse nature of the spray flow is captured whilst only considering the liquid as one phase. The first four moments of the droplet number distribution have been found to provide an adequate representation of the poly-disperse nature of the spray, and by solving equations for these parameters, a fully multi-size model of the spray has been constructed. The number of equations to be solved is significantly fewer than in either of the previous poly-disperse spray models making the scheme more computationally efficient than its predecessors. The use of these moments means that the spray is dealt with in terms of average quantities, allowing a smooth representation of the droplet size distribution at all points, rather than a discrete representation. This is an advantage even when considering phenomena such as droplet break-up in which a discrete representation of the outcome of the break-up would seem most appropriate, for it is not the break-up process itself which is important but rather its effect on the overall size distribution of the spray. This latter quantity should remain smooth. These distribution function moments are very useful parameters in characterising the spray as they are inherently related to the spray mean diameters. They are also the terms needed in order to produce the source terms for the effects of the spray on the gas phase when considering the spray as a whole (Beck, 2000; Beck and Watkins, 2002, 2003).

2. Model formulation

2.1. Drop number probability distribution moments

The moments of the drop number probability distribution are defined by

$$Q_i = \int_0^\infty n(r) r^i \, \mathrm{d}r, \tag{1}$$

where $n(r)$ is the fraction of droplets having radii between limits $r + \mathrm{d}r/2$ and $r - \mathrm{d}r/2$.

In the new model the first four moments, Q_0 to Q_3 are used. At a particular point in space and time, Q_0 is the total number of drops present, Q_1 is the total sum of radii of the drops, $4\pi Q_2$ is the total surface area of the drops and $4\pi Q_3/3$ is the total volume of the drops.

Mean droplet diameters are often used to characterise the droplet sizes in a spray; these four parameters provide all mean droplet diameters from D_{10} to D_{32}, as by definition,

$$D_{pq}^{p-q} = \frac{2^{p-q} Q_p}{Q_q}. \tag{2}$$

Hence it can be seen that these parameters contain a great deal of information about the spray. In many respects the most important of the four moments is Q_3, as assuming that locally all droplets have the same density, this parameter defines the mass of liquid present per unit volume. This means that the transport equation for Q_3 is equivalent to a liquid phase continuity equation. This suggests strongly that any modelling done using these moments must at least consider this fourth moment, and it has been shown in earlier publications that the modelling of important spray phenomena also require values for the other three.

2.2. Moment–average quantities

Previous publications of the model have also demonstrated that to write Eulerian transport equations for the droplet moments, the mean speed at which the moments are convected has to be defined and that the mean speed must be different for each of the moments. Logically the net convection of mass should occur at the mass–average velocity, and the net convection of droplet surface area (say) should occur at the surface-area–average velocity, and there is no reason for these two values to be the same. Larger droplets experience less drag and generally have higher velocities than the smaller droplets. This effect is modelled by ensuring that the mass–average velocity is higher than the surface-area–average velocity. The moment–average liquid velocity vector $U_{\mathrm{l}i}$ averaged over the ith moment Q_i is defined as

$$U_{\mathrm{l}i} = \frac{\int_0^\infty r^i n(r) U_{\mathrm{l}} \, \mathrm{d}r}{Q_i}. \tag{3}$$

From the definitions of the droplet moments, the mass–average velocity is the correct velocity at which to convect Q_3 and the surface-area–average velocity is the correct velocity at which to convect Q_2. The same idea can also be applied to moment–average energies to capture the effect of small droplets heating up more quickly than large droplets, although this approach has not yet been implemented in the model.

The result of defining both the drop number moments and the moment-averaged velocities is that the former provide a representation of the distribution of droplet sizes at each point in space and time, while the latter provide the means by which the distribution of droplet sizes can change in space and time. The two concepts allied together are capable of providing a picture of the behaviour of a poly-disperse spray.

This model is not concerned with knowing the precise velocity of every droplet, as is the case in the DDM, but uses a selection of average velocities and their relationship to each other to determine how the size distribution evolves at each point in space and time. The key question is whether this continuum averaging gives as good a representation of the spray and its dynamics as can be obtained by discretising the droplets into size groups. Ample evidence has been provided by earlier publications that the answer to this question is yes.

2.3. Liquid phase transport equations

The transport equation for the fourth drop number moment is written as the liquid mass conservation equation

$$\frac{\partial}{\partial t}(\rho_l(1-\theta)) + \frac{\partial}{\partial x_j}(\rho_l(1-\theta)U_{l3j}) = -S_m. \tag{4}$$

The void fraction, θ, which is the volume fraction of gas in each computational grid cell, is given by

$$\theta = 1 - \frac{V_l}{V_{cell}} = 1 - \frac{4\pi Q_3}{3}. \tag{5}$$

Thus θ can be calculated directly from the fourth moment of the droplet number distribution function. The convection velocity vector required is the appropriate moment–average value U_{l3}. The source term S_m in Eq. (4) has only one contribution due to evaporation, as the other phenomena considered in the model do not affect the total mass of liquid present.

The equations for the remaining moments take a similar form, but more source terms must be included due to the changes effected by droplet break-up, droplet–droplet collisions, evaporation, and changes in the droplet density. The equations are

$$\frac{\partial}{\partial t}(Q_i) + \frac{\partial}{\partial x_j}(Q_i U_{lij}) = -S_{Q_i}. \tag{6}$$

Use of the ith moment–average velocity in these equations should be noted. In the present version of the model, these equations are solved only for $i = 2$, i.e. for the surface-area moment, for reasons explained in Section 3.2.

The liquid phase momentum equation, as used in the calculation scheme, is derived in Beck and Watkins (2003) and is written as

$$\begin{aligned}&\frac{\partial}{\partial t}(\rho_l(1-\theta)U_{l3i}) + \frac{\partial}{\partial x_j}(\rho_l(1-\theta)U_{l3i}U_{l3j}) + U_{l3i}S_m \\ &\quad = \frac{\partial}{\partial x_j}\left(\rho_l(1-\theta)\sigma_v \nu_l \frac{\partial U_{l3i}}{\partial x_j}\right) - S_{U_i},\end{aligned} \tag{7}$$

where σ_v is the coefficient of Melville and Bray (1979).

The equations for the other moment–average velocities follow the same pattern,

$$\begin{aligned}&\frac{\partial}{\partial t}(Q_k U_{lkj}) + \frac{\partial}{\partial x_j}(Q_k U_{lki}U_{lkj}) + \frac{\partial}{\partial x_j}(Q_k(U_{l3i} - U_{lki}) \\ &\qquad \times (U_{l3j} - U_{lkj})) + U_{l3i}B_{Q_i} + U_{lki}(S_{Q_i} - B_{Q_i}) \\ &\quad = \frac{\partial}{\partial x_j}\left(Q_k \sigma_v \nu_l \frac{\partial U_{lki}}{\partial x_j}\right) - S_{U_{ki}},\end{aligned} \tag{8}$$

but there are important differences, notably the third term on the left hand side of Eq. (8). The reasons for the existence of this term are given in Beck and Watkins (2003). Again, this equation is solved only for $k = 2$ in the present version of the model.

The liquid phase energy equation is more simply derived as the temperature of the droplets in a region of space is, in the present version of the model, considered to be independent of the droplet radius. The equation is written as

$$\begin{aligned}&\frac{\partial}{\partial t}(\rho_l(1-\theta)E_l) + \frac{\partial}{\partial x_j}(\rho_l(1-\theta)U_{l3j}E_l) + E_l S_m \\ &\quad = \frac{\partial}{\partial x_j}\left(\rho_l(1-\theta)\sigma_v \nu_l \frac{\partial E_l}{\partial x_j}\right) - S_E.\end{aligned} \tag{9}$$

The source terms relating to the hydrodynamics of the spray in Eqs. (6)–(9) are discussed in detail in Beck and Watkins (2002), so the derivation of these will not be considered further here, but they are quoted in Section 3.3 for completeness. Those source terms in Eqs. (4) and (6)–(9) relating to the heat and mass transfer processes are the subject of this publication and therefore their derivations are discussed in detail in Section 3.4.

2.4. Gas phase transport equations

The gaseous mass transport equation is written as

$$\frac{\partial}{\partial t}(\theta\rho_g) + \frac{\partial}{\partial x_j}(\theta\rho_g U_{gj}) = S_m, \tag{10}$$

where S_m is the mass transferred from the liquid phase to the gas phase per unit time within a control volume.

The gaseous momentum equation, including turbulence effects, is written as

$$\begin{aligned}&\frac{\partial}{\partial t}(\theta\rho_g U_{gi}) + \frac{\partial}{\partial x_j}(\theta\rho_g U_{gj}U_{gi}) \\ &\qquad - U_{gi}\left(\frac{\partial}{\partial t}(\theta\rho_g) + \frac{\partial}{\partial x_j}(\theta\rho_g U_{gj})\right) \\ &\quad = \frac{\partial}{\partial x_j}\left(\mu_{eff}\theta\left(\frac{\partial U_{gi}}{\partial x_j} + \frac{\partial U_{gj}}{\partial x_i}\right)\right) - \theta\frac{\partial P}{\partial x_i} \\ &\qquad - \frac{\partial}{\partial x_j}\left(\frac{2}{3}\theta\rho_g k\delta_{ij}\right) + S_m(U_{li} - U_{gi}) + S_{U_i}.\end{aligned} \tag{11}$$

The effective viscosity, μ_{eff}, is given by

$$\mu_{eff} = \mu_{lam} + \rho_g C_\mu \frac{k^2}{\varepsilon}, \tag{12}$$

where C_μ is taken to be a constant equal to 0.09. The source term S_{U_i} in Eq. (11) is the momentum exchanged from the liquid to the gas per unit time in a control volume.

Similarly, the gaseous stagnation energy transport equation, including the mass transfer term, is written as

$$\frac{\partial}{\partial t}(\theta\rho_g E_g) + \frac{\partial}{\partial x_j}(\theta\rho_g U_{gj} E_g) - E_g S_m = \frac{\partial}{\partial x_j}\left(\frac{\mu_{eff}}{\sigma_t}\theta\left(\frac{\partial E_g}{\partial x_j}\right)\right) - \theta\frac{\partial}{\partial x_j}(PU_{gj}) + S_E, \quad (13)$$

where S_E is the inter-phase energy transfer. The evaporation model requires that the properties of the spray vapour be taken into account. Hence a transport equation for the vapour mass fraction f must be solved. This is formulated as

$$\frac{\partial}{\partial t}(\theta\rho_g f) + \frac{\partial}{\partial x_j}(\theta\rho_g U_{gj} f) - f S_m = \frac{\partial}{\partial x_j}\left(\mu_{eff}\theta\left(\frac{\partial f}{\partial x_j}\right)\right) + S_m. \quad (14)$$

This effectively changes the properties of the carrier gas. The state equation becomes

$$P = \rho_g R_{mix} T_g, \quad (15)$$

where

$$R_{mix} = R_0\left(\frac{1-f}{M_a} + \frac{f}{M_v}\right). \quad (16)$$

The specific heat capacity of the mixture is given by

$$c_{p,mix} = \frac{(1-p_r)M_a c_{p,a} + p_r M_v c_{p,v}}{(1-p_r)M_a + p_r M_v}, \quad (17)$$

where the ratio of the average partial pressure of the vapour to the total pressure is given by

$$p_r = \frac{P_v}{2P}. \quad (18)$$

The turbulence model employed is a two-equation model, the equations being solved for the turbulence kinetic energy k, and its dissipation rate ε. The equations are

$$\frac{\partial}{\partial t}(\theta\rho_g \mathrm{k}) + \frac{\partial}{\partial x_j}(\theta\rho_g U_{gj}\mathrm{k}) - \mathrm{k}S_m = \frac{\partial}{\partial x_j}\left(\frac{\mu_{eff}}{\sigma_k}\theta\left(\frac{\partial \mathrm{k}}{\partial x_j}\right)\right) + \theta P_k - \rho_g\varepsilon\theta \quad (19)$$

and

$$\frac{\partial}{\partial t}(\theta\rho_g\varepsilon) + \frac{\partial}{\partial x_j}(\theta\rho_g U_{gj}\varepsilon) - \varepsilon S_m = \frac{\partial}{\partial x_j}\left(\frac{\mu_{eff}}{\sigma_\varepsilon}\theta\left(\frac{\partial\varepsilon}{\partial x_j}\right)\right) + \theta C_{\varepsilon 1}P_k\frac{\varepsilon}{\mathrm{k}} - \theta C_{\varepsilon 2}\frac{\rho_g\varepsilon^2}{\mathrm{k}} + \theta C_{\varepsilon 3}\rho_g\varepsilon\frac{\partial U_{gj}}{\partial x_j}. \quad (20)$$

The turbulence kinetic energy production rate is given by

$$P_k = \rho_g C_\mu\frac{\mathrm{k}^2}{\varepsilon}\left(\frac{\partial U_{gi}}{\partial x_j} + \frac{\partial U_{gj}}{\partial x_i}\right)\frac{\partial U_{gj}}{\partial x_i}. \quad (21)$$

The constants take the values $C_{\varepsilon 1} = 1.44$, $C_{\varepsilon 2} = 1.92$, $C_{\varepsilon 3} = -0.373$, $\sigma_t = 0.9$, $\sigma_k = 1.0$, $\sigma_\varepsilon = 1.3$. The term involving $C_{\varepsilon 3}$ is an addition due to the effect of the liquid phase on the gas phase turbulence. All the source terms in Eqs. (10), (11), (13) and (14) are calculated by considering the effect of the gas phase on the liquid phase in terms of the droplet number distribution function moments. As already noted above, these are discussed in Section 3, particularly where they relate to heat and mass transfer.

2.5. Computational solution

The spray test cases studied in this paper are axisymmetric, thus here the equations are solved on a two-dimensional axisymmetric orthogonal computational grid. Euler implicit temporal differencing and hybrid upwind/central spatial differencing are employed. Discussion of these issues and the algorithm used can be found in Beck and Watkins (2002).

3. Spray sub-models

To form a complete simulation of spray behaviour, many phenomena found in sprays require modelling. In general, these models are more naturally described in a Lagrangian framework, and hence the majority are written in this form, although all are incorporated into a Eulerian frame within the model. The Eulerian models described in the literature tend to consider dilute sprays, for which many of these phenomena can be neglected, as it is conceptually more difficult to write the sub-models in this form, especially those for droplet break-up and collisions.

3.1. Inlet conditions

Although not strictly a sub-model, a brief discussion of the inlet conditions is given here for completeness. The applications of the model made to date assume the spray to be fully atomised within a few (normally one or two) grid cells from the nozzle exit. This is not an essential feature of the model, as a drop break-up sub-model could equally well be used to atomise the inlet liquid, as is often done in DDM applications. The modelling of the spray injection is based on the injection cell treatment of Watkins (1989). The injector is located within this cell or cells, and it is assumed that the gas has entrained to the liquid velocity by the downstream face

of the cell(s). The velocities and void fraction are calculated there by one-dimensional inviscid flow analysis. Some minor adjustments have been made to the basic injection cell concept for this spray model, and it has been applied to both solid cone and hollow cone sprays.

The main difference in this work from the injection cell treatment of Watkins (1989) is that the injection domain is comprised of more than one cell. The main reason for this is that it allows a greater range of radial velocities to be applied to the spray at inlet, given that the liquid velocities are applied at cell faces, and that there are no droplet groups. The fineness of grid with which this model is able to work allows the injection domain to be comprised of a number of cells (up to five radial cells have been used successfully), and yet be smaller than the injection domain used in most DDM calculations. An advantage of the axisymmetric grid being used in the present applications is that if the spray is approximately conical in the injection cell(s), the radial size of the domain can be chosen such that the spray is exactly fitted into the injection cell(s) domain at the downstream face. This results in removal of the over-prediction of the amount of gas being entrained that is a problem when using axisymmetric grids with DDMs. A schematic of the injection domain for a full cone spray is presented in Fig. 1. The equations solved in order to produce the downstream values of velocity components and void fraction, for both full cone and hollow cone sprays, are presented in Beck and Watkins (2002), so will not be repeated here.

Using the calculated value of the void fraction at the downstream face of the injection domain, the value of Q_3 can be calculated via Eq. (5). The value of Q_2 is then calculated from a prescribed inlet Sauter mean radius (SMR), and the other two moments can then be calculated from a truncated form of the assumed distribution, as described in the next sub-section. For each direction, all the moment-averaged velocity components are assigned the same value, calculated as outlined above.

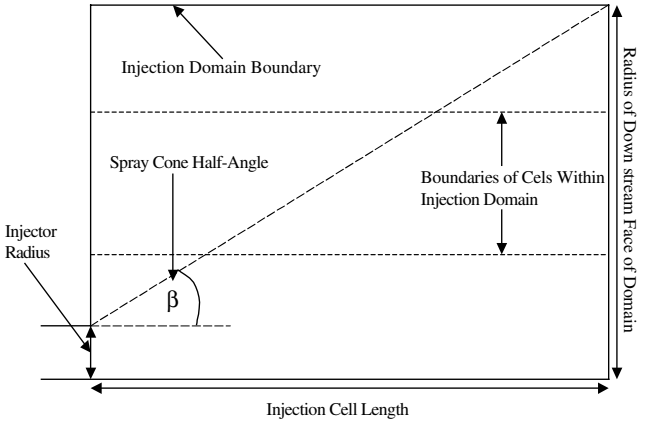

Fig. 1. Injection domain and parameters for a solid cone spray.

3.2. Droplet number distribution assumptions

Accurate representation of the spectrum of droplet sizes is essential in the modelling of poly-disperse sprays. Initially the calculation scheme was intended to provide enough information about the droplet size distribution to model the spray by predicting the first four moments of the number distribution function from transport equations. The break-up and collisions models require a means of predicting the surface area or total radius of part of the distribution, and not the whole. The only way to do this is to produce a function that approximates the droplet number distribution function, and has moments that match those provided by the distribution function. As the model allows the four moments to be transported at different velocities, the poly-disperse nature of the flow can be simulated. This, however, brings its own problems. Unless the moments tend towards having similar velocities at the edge of the spray, the droplet sizes at the periphery quickly become either very large or very small causing the numerical scheme to become unstable. It has proved too great a task to date to ensure that all four velocities are similar enough at the spray edges for the scheme to be reliable in most cases. Instead transport equations are solved for fewer than four moments, and hence fewer moment–average velocities. Using the calculated moments an approximate distribution function is derived from which the remaining moments are evaluated. This has two advantages over the four-moment approach. Firstly, there are fewer moment–average velocities allowing a greater likelihood of being able to keep the scheme stable at the spray periphery, and fewer transport equations are being solved which reduces the amount of computational work done. To date only a two-moment scheme has been successfully applied.

The SMR is generally considered the most important parameter in the size distribution function, and so it would seem sensible to use the SMR as the parameter required in a two-moment distribution function. Other desirable qualities in this distribution function are accurate representation of typical droplet size distributions and ease of analytic integration in order to avoid having to perform numerical integrations.

An analytically integrable function to use as a number distribution was sought such that the volume distribution it produced was a reasonable approximation to a Rosin–Rammler distribution. The Rosin–Rammler volume distribution is commonly applied in sprays, particularly for solid-cone diesel sprays. It is defined by

$$v(r) = \left(\frac{\alpha_R}{r_R^{\alpha_R}}\right) r^{\alpha_R - 1} \exp\left(-\left(\frac{r}{r_R}\right)^{\alpha_R}\right), \tag{22}$$

where r_R is known as the Rosin–Rammler mean radius, and α_R the Rosin–Rammler exponent. r_R is the droplet radius for which 63% of the liquid mass is made up of

droplets with smaller radii. The exponent determines the shape of the distribution, and the majority of sprays have distributions with exponents between the values of 2 and 4, and mostly at the lower end of this range, as reported by Wang and Lefebvre (1987). Thus it was chosen to match a Rosin–Rammler distribution of exponent 2. The number distribution found to do this is

$$n(r) = \frac{16r}{\bar{r}_{32}^2} \exp\left(-\frac{4r}{\bar{r}_{32}}\right), \tag{23}$$

where the SMR $\bar{r}_{32}$ is used as all the droplet moments are defined in terms of the droplet radii. The comparison of the volume distribution produced by this approximation with the Rosin–Rammler distribution is made in Fig. 2. This shows that the volume of very small droplets is slightly less in the new distribution compared to the Rosin–Rammler distribution and the volume of mid-range droplets is greater. However, the distributions match excellently for large droplets. The new distribution is a good enough approximation to be at least as good a representation of the Rosin–Rammler distribution as produced by a discretisation into separate droplet groups, unless a very large number of groups is considered.

The approach used is to consider the initial full distribution as a reference distribution based on a reference SMR which is invariant, and changes in the local SMR are obtained by truncating the distribution to match the SMR as predicted by the transport equations for Q_3 and Q_2. Values of SMR larger than the reference value are obtained by removing the small droplets from the distribution, and SMR values smaller than the reference value are obtained by removing the large droplets from the distribution. The other two moments can then be found from this truncated distribution. This model is equivalent to assuming that the change in the droplet size distribution is due to only larger droplets being convected into some regions of the spray and only small droplets reaching other regions. The key reason for choosing this approach is that the truncated distribution tends towards having mono-disperse behaviour whichever end is being truncated. Therefore, once a certain droplet size is reached at the spray periphery, the moment–average velocities can be considered to be identical, and hence the instability problems can be completely solved.

The truncated distribution is also used to provide the number, total radius, and sum of squares of radii of droplets undergoing break-up and collisions. Details of how this is achieved can be found in Beck (2000). The manner in which these variables are applied into the hydrodynamic source terms of the conservation equations is set out in detail in Beck and Watkins (2002), but the final forms are also given here for completeness.

3.3. Hydrodynamic inter-phase source terms

The final derivations depend on the details of the sub-models employed. For example, in the current applications of the model the drag on the drops is modelled as for solid spheres, and the momentum source terms become

$$S_{U_{3j}} = 6\pi\mu_g U_{\mathrm{rel},j} Q_1 + 1.8\pi(\rho_g |U_{\mathrm{rel}}| Q_2)^{0.687} \left(\frac{\mu_g Q_1}{2}\right)^{0.313} U_{\mathrm{rel},j}. \tag{24}$$

A different source term would be obtained if, e.g., drops were modelled as oscillating between spheres and discs. This latter model has not been implemented to date, but

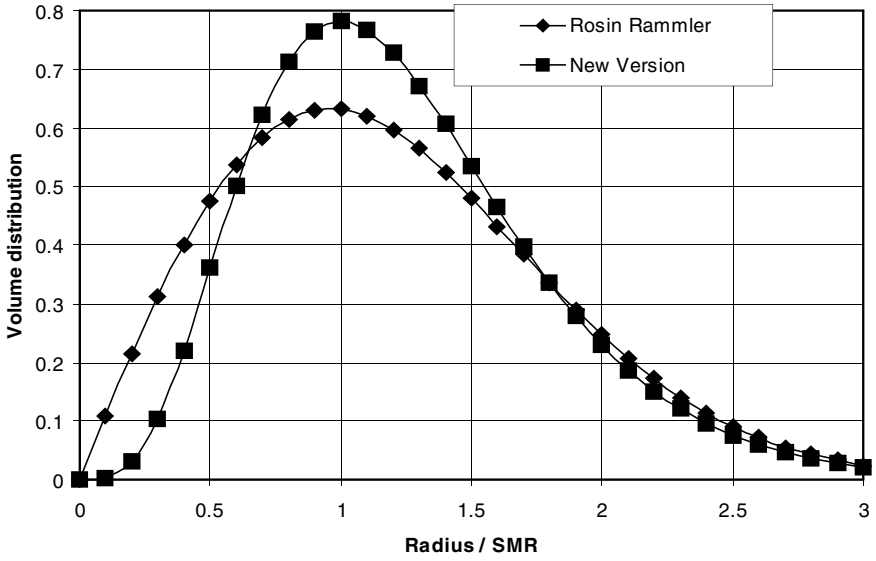

Fig. 2. Comparison of simplified distribution used in the model with the Rosin–Rammler distribution of exponent 2.

there is no intrinsic reason to prevent its use within the present modelling approach.

A similar derivation is performed for the liquid surface-area–average velocity source term. This source term is given by

$$S_{U_{2j}} = \frac{9}{2}\frac{Q_0}{\rho_l} U_{\mathrm{rel},j}\mu_g + \frac{1.35}{\rho_l} U_{\mathrm{rel},j}\left(\frac{\mu_g Q_0}{2}\right)^{0.313} (|U_{\mathrm{rel}}|\rho_g Q_1)^{0.687}. \quad (25)$$

The droplet break-up model accounts for the effects on the droplet distribution function moments of the break-up of unstable droplets. There are generally considered to be three types of droplet instability (Liu and Reitz, 1993) they can undergo bag break-up, stripping break-up and surface wave break-up. The last of these is mainly seen in the initial atomisation of the spray, and so the models used to date only consider the other two. These are straightforward in nature and have been used in many DDM codes. For stripping break-up, the change in the surface area per unit time for a single droplet is given by

$$S_{Q_2,\mathrm{s}} = \frac{(Q_{2,\mathrm{s}}Q_{1,\mathrm{s}})^{\frac{1}{2}}}{6.2\left(\frac{\rho_l}{\rho_g}\right)^{\frac{1}{4}}\left(\frac{\mu_l}{2\rho_l U_{\mathrm{rel}}}\right)^{\frac{1}{2}}\frac{r_s}{U_{\mathrm{rel}}}\left(\frac{\rho_l}{\rho_g}\right)^{\frac{1}{2}}} - \frac{Q_{1,\mathrm{s}}}{\frac{r_s}{U_{\mathrm{rel}}}\left(\frac{\rho_l}{\rho_g}\right)^{\frac{1}{2}}} \quad (26)$$

and $Q_{1,\mathrm{s}}$ and $Q_{2,\mathrm{s}}$ are the total radius and total sum of squares of radii of drops undergoing stripping break-up.

For bag break-up, no appropriate correlation has been found in the literature, and so the surface area is assumed to double in the break-up, which is equivalent to the production of eight equally sized droplets. Thus the term becomes

$$S_{Q_2,\mathrm{b}} = \frac{(Q_{0,\mathrm{b}}Q_{1,\mathrm{b}})^{\frac{1}{2}}}{\pi\left(\frac{\rho_l}{2\sigma}\right)^{\frac{1}{2}}}. \quad (27)$$

$Q_{1,\mathrm{b}}$ and $Q_{0,\mathrm{b}}$ represent the total radius and total number of the droplets undergoing bag break-up.

The latter two source term contributions to the change in the third droplet distribution moment are then summed to give the total change in the moment due to break-up. As this model only provides a value for the change in the third droplet moment, it is only appropriate for use when transport equations are being solved for only the third and fourth moments, and the other two approximated from a presumed distribution.

The collisions model is semi-empirical, and has three stages. The first stage is to determine the number of collisions between droplets occurring in any control volume. This is based on the collision frequency concept of O'Rourke and Bracco (1980). This approach to collision modelling is also followed in many DDMs. In the current model the number of collisions is given by

$$N_{\mathrm{coll}} = C_{\mathrm{coll}}\pi U_{\mathrm{rel}}(Q_0 Q_2 + Q_1^2), \quad (28)$$

where C_{coll} is a model constant introduced due to the prediction of large numbers of collisions with this model. It is usually taken as 0.15. The relative velocity between droplets is approximated by assuming that the large droplets are travelling at approximately the mass–average velocity, and the small droplets have been fully entrained to the gas velocity. This means that the average droplet–droplet relative velocity is approximated as one half of the relative velocity between the mass–average liquid velocity and the local gas velocity.

The second stage of the model determines how many of these collisions result in each of the regimes of coalescence, bounce and separation, described by Orme (1997). The two parameters required to determine these numbers are the Weber number, defined as

$$We = \frac{2r\rho_l U_{\mathrm{rel}}}{\sigma} \quad (29)$$

and the impact parameter, b. The impact parameter is defined as the perpendicular distance from the centre of one droplet to the relative velocity vector placed on the centre of the other droplet at impact, normalised by the sum of the radii. Jiang et al. (1992) provide a map of the different collision regimes on a graph of Weber number against impact parameter. Their original chart for hydrocarbon droplets is simplified for the purposes of the present model as shown in Fig. 3. The thresholds between regimes are slightly dependent on the ambient pressure. However, this effect has been neglected to date. The chart used is based on an ambient pressure of 0.1 MPa. A similar chart has also been used for water droplets (Beck (2000)).

The critical Weber numbers shown on the chart are translated into critical radii, and an assumed distribution is used to determine the probability that any given droplet lies between adjacent critical radii. The outcome of a collision depends mainly on the Weber number of the *smaller* droplet, according to Orme (1997), and the impact parameter. For the hydrocarbon droplets, there

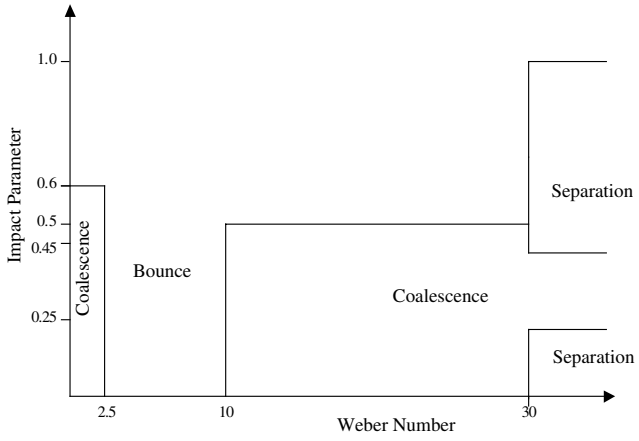

Fig. 3. Simplified schematic of collision regimes transition criteria for hydrocarbon droplets.

exist three critical radii, and the probability that the smaller radius of the two colliding droplets falls between given critical radii is determined from the chart. The total coalescence probability for hydrocarbon droplets is given as the sum of the probabilities of the drops falling within the different ranges for coalescence. The probability of separation after collision is also derived from the chart.

The final stage of the collisions model is to determine the effect of the predicted collisions on the droplet moments, specifically the surface area, as the liquid mass is conserved during the collision. The surface area change is modelled as being equal to that obtained from a collision between two droplets of equal radius and to result in either one (coalescence) or five (separation) droplets, also of equal radius, such that the droplet volume is conserved. The effect of changing the number of droplets produced in separation has not been tested. The inlet droplet size, r, is dependent on the inlet Weber number, and the values it takes for each regime are presented in Table 1 for hydrocarbon droplets, along with the change in the square of the radius, δQ_2, resulting from the collision. The source term for the surface area moment is

$$S_{Q_2,\mathrm{coll}} = N_{\mathrm{coll}}(\mathrm{P}_{\mathrm{coll,a}}\delta Q_{2,\mathrm{a}} + \mathrm{P}_{\mathrm{coll,b}}\delta Q_{2,\mathrm{b}} + \mathrm{P}_{\mathrm{coll,c}}\delta Q_{2,\mathrm{c}} + \mathrm{P}_{\mathrm{sep}}\delta Q_{2,\mathrm{sep}}) \tag{30}$$

for hydrocarbon droplets. Similar equations and tables have been produced by Beck (2000) for water droplet collisions.

3.4. Heat and mass transfer source terms

In this section those source terms in the conservation equations that specifically relate to the evaporation processes are described and derived in detail. These have previously only been presented in Beck (2000).

The mass lost from a single droplet is

$$\dot{m} = 2\pi r\left(\frac{k}{c_p}\right)_{\mathrm{g}} Sh, \tag{31}$$

where Sh is the Sherwood number. For quiescent conditions $Sh = 2$. However, for moving drops an additional contribution due to turbulent convection is required. Two forms of the Sherwood number for such conditions have been proposed. The first is based on the Spalding (1953) mass transfer number, defined

$$B_{\mathrm{M}} = \frac{f_{\mathrm{s}}}{1 - f_{\mathrm{s}}}, \tag{32}$$

where subscript s refers to the drop surface conditions. Then the Sherwood number is defined by

$$Sh = 2\ln(1 + B_{\mathrm{M}}). \tag{33}$$

An alternative form of Sh is given by a correlation, as e.g. Ranz and Marshall (1952):

$$Sh = 2\left(1 + 0.3Re^{\frac{1}{2}}Sc^{\frac{1}{3}}\right), \tag{34}$$

where Re is the Reynolds number, given by

$$Re = \frac{2\rho_{\mathrm{g}} r|U_{\mathrm{rel}}|}{\mu_{\mathrm{g}}} \tag{35}$$

and $Sc = ((\mu/\rho\Gamma))_{\mathrm{g}}$ is the Schmidt number.

For the model presented here, the first form of the Sherwood number has been used. However, use of the alternative form is under investigation.

Then

$$\dot{m} = 4\pi r\left(\frac{k}{c_p}\right)_{\mathrm{g}} \ln(1 + B_{\mathrm{M}}). \tag{36}$$

Eq. (36) can be integrated over all droplets at a local level to obtain the desired mass source term. The result is

$$S_{\mathrm{m}} = 4\pi\left(\frac{k}{c_p}\right)_{\mathrm{g}} \ln(1 + B_{\mathrm{M}})Q_1. \tag{37}$$

The source term for the liquid surface area equation can also be derived from the same starting point. The loss in mass can be related to a change in radius by

$$\delta m = \rho_{\mathrm{l}} 4\pi r^2 \delta r. \tag{38}$$

The change in the square of the droplet radius is related to the droplet radius change via

$$\delta(r^2) = 2r\delta r. \tag{39}$$

Thus the change in the square of the droplet radius per unit mass lost is

$$\frac{\delta(r^2)}{\delta m} = \frac{1}{2\pi\rho_{\mathrm{l}} r}. \tag{40}$$

Using Eq. (36), the change in the square of the radius can then be written as

$$\frac{\partial(r^2)}{\partial t} = \frac{2}{\rho_{\mathrm{l}}}\left(\frac{k}{c_p}\right)_{\mathrm{g}} \ln(1 + B_{\mathrm{M}}). \tag{41}$$

Table 1
Determination of surface area change for collisions between hydrocarbon droplets

	Inlet droplet radius, r	Change in square of radius
$r_{\mathrm{smaller}} < r_{\mathrm{a}}$	r_{a}	$\delta Q_{2,\mathrm{a}} = (2^{2/3} - 2)r^2 = -0.41r^2$
$r_{\mathrm{b}} < r_{\mathrm{smaller}} < r_{\mathrm{c}}$	$0.5(r_{\mathrm{b}} + r_{\mathrm{c}})$	$\delta Q_{2,\mathrm{b}} = (2^{2/3} - 2)r^2 = -0.41r^2$
$r_{\mathrm{smaller}} > r_{\mathrm{c}}$ (Coalescence)	r_{c}	$\delta Q_{2,\mathrm{c}} = (2^{2/3} - 2)r^2 = -0.41r^2$
$r_{\mathrm{smaller}} > r_{\mathrm{c}}$ (Separation)	r_{c}	$\delta Q_{2,\mathrm{sep}} = (5(0.4)^{2/3} - 2)r^2 = 0.71r^2$

Integrating Eq. (41) over all droplets locally, the contribution to the source term for Q_2 from the change in mass is given by

$$S_{Q_2,\mathrm{evap}} = \frac{2}{\rho_\mathrm{l}}\left(\frac{k}{c_p}\right)_\mathrm{g} \ln(1+B_\mathrm{M})Q_0. \tag{42}$$

The heat transferred between phases during the heat-up period when the liquid is not at saturation temperature is given by

$$Q_\mathrm{in} - Q_\mathrm{evap} = 2\pi r k_\mathrm{g}\left[Nu(T_\mathrm{g} - T_\mathrm{l}) - Sh\frac{L}{c_{pg}}\right], \tag{43}$$

where L is the latent heat of vaporisation for the liquid and Nu is the Nusselt number.

For quiescent conditions, $Nu = 2$. For turbulent convective conditions, again two forms have been proposed. The first employs the heat transfer number, expressed in terms of the mass transfer number by

$$Nu = 2\frac{\ln(1+B_\mathrm{M})}{B_\mathrm{M}}. \tag{44}$$

The alternative form employs a correlation, such as that due to Ranz and Marshall (1952):

$$Nu = 2\left(1 + 0.3Re^{\frac{1}{2}}\sigma^{\frac{1}{3}}\right), \tag{45}$$

where $\sigma = (c_p\mu/k)_\mathrm{g}$ is the Prandtl number. For the model presented here, the first form has been employed. Then

$$Q_\mathrm{in} - Q_\mathrm{evap} = 4\pi r k_\mathrm{g}\ln(1+B_\mathrm{M})\left[\frac{T_\mathrm{g} - T_\mathrm{l}}{B_\mathrm{M}} - \frac{L}{c_{pg}}\right]. \tag{46}$$

This equation can be integrated locally over all droplets to give

$$S_\mathrm{E} = -4\pi k_\mathrm{g}\ln(1+B_\mathrm{M})\left[\frac{T_\mathrm{g} - T_\mathrm{l}}{B_\mathrm{M}} - \frac{L}{c_{pg}}\right]Q_1. \tag{47}$$

Note the presence of the minus sign due to the source term being the energy gained by the gas phase in Eq. (13), and lost by the liquid phase in Eq. (9). Care must be taken when the temperature difference is very small, but the liquid is super-saturated. For this type of mass transfer, it is assumed that the liquid gains from the gas exactly the energy it requires to evaporate the appropriate amount of mass. Hence the source term S_E becomes zero in this case as the net transfer of energy to the liquid is exactly zero.

The source terms for mass (Eq. (37)), momentum (Eqs. (24) and (25)) and energy (Eq. (47)) are calculated directly and can thus be straightforwardly implemented into the corresponding conservation equations ((4), (7), (8) and (9) for the liquid phase and (10), (11), (13) and (14) for the gas phase). The equation for the liquid surface area is less simple as it has many contributions, from bag break-up, stripping break-up, collisions and mass transfer. The source term used in Eq. (6) is the sum of these, given by Eqs. (26), (27), (30), and (42), respectively,

$$S_{Q_2} = S_{Q_2,\mathrm{b}} + S_{Q_2,\mathrm{s}} + S_{Q_2,\mathrm{coll}} + S_{Q_2,\mathrm{evap}}. \tag{48}$$

4. Test cases

A number of test cases involving non-evaporating sprays have previously been simulated using the new model and the results are presented in Beck and Watkins (2002, 2003). Those publications have demonstrated the basic soundness of the new approach. They included test cases that have allowed all the hydrodynamic sub-models to be tested, including the drag, drop break-up and drop collision sub-models. Also tested were the inlet conditions, assumed size distribution approach, and numerical aspects, such as the effects of grid size spacing and time steps.

Beck (2000) also calculated a number of evaporating sprays, and it is this work that is reported on here. The behaviour of evaporating sprays is of much interest in many engineering problems. Combustion in gas turbines and in internal combustion engines is strongly controlled by the dynamics of the injected spray. The evaporation of the spray is a vital part of this process, as it is the spray vapour that burns. Hence, for a numerical model to be useful in the design process, both the spray structure and the evaporation of droplets require accurate modelling.

The performance of the model in predicting evaporation is tested both in a series of parametric tests, and in comparison with experimental data. Unfortunately there is a dearth of useful data on evaporating sprays in the literature that can be utilised for validating the model performance. The experiments of Solomon et al. (1985) described later are the most reliable and well presented set of evaporative spray data found, and considered likely to be the most valid test of the model performance. However, before examining the abilities of the model to quantitatively match experimental data, the qualitative abilities are examined through parametric explorations.

5. Results and discussion

5.1. Parametric tests

The parametric tests are based on the test conditions of Levy et al. (1997). These tests are designed to ensure that the model captures all effects on the spray due to evaporation. In the tests, a diesel spray is injected at 17 MPa and room temperature into a cylindrical chamber of 80 mm diameter at an ambient pressure of 2 MPa. In the base case the ambient gas temperature is 659 K. The

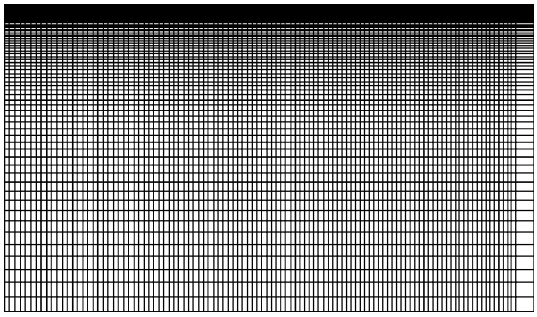

Fig. 4. Grid used for the parametric tests. The domain is 100 mm long by 80 mm in radius with 109×73 cells.

nozzle has radius 0.1 mm and the spray angles are calculated via correlations (Ranz, 1958). The simulations are run using a time step of 2 μs and an injection cell of largest side 1 mm. The complete grid used is presented in Fig. 4. A similar grid structure is used for all the test cases presented in this paper. As discussed later in this paper, tests have been carried out to ensure the time step and grid independence of the results. Thus effects such as numerical diffusion caused by the first order nature of the spatial discretisation scheme employed, are at least partially eliminated. The inlet and reference droplet SMR are both 7 μm. The results presented are the droplet SMR obtained by considering all droplets at a given axial distance from the nozzle, and the centreline vapour mass fraction. Both are instantaneous results obtained after 5 ms.

The basic structure of a narrow solid cone evaporating spray is similar to that of a narrow cone non-evaporating spray, as presented in Beck and Watkins (2003). The structural analysis of evaporating sprays concentrates on the effects of heat transfer, considering the distributions of gaseous temperature and vapour mass fraction. Beck (2000) demonstrates that the hot ambient gas provides heat for the liquid and is cooled in the region where droplets exist, with the lowest temperatures being found along the centreline where the liquid volume is the highest. The lowest gas temperatures are found at the front of the spray highlighting the large amount of heat taken from the gas in order to facilitate the evaporation of the liquid droplets, and that the time the liquid has spent in the gaseous environment largely determines the temperature of its surroundings. The distributions of vapour mass fraction support these observations; these show that the vapour mass fraction is very low in the near nozzle region due to the low temperature of the injected liquid. The droplets then heat up, which increases the rate of evaporation, and hence the vapour mass fraction increases towards the spray tip as these droplets have had the longest heating time. The higher evaporation rates that are seen at the very forward edge of the spray correlate to the lowest observed gas temperatures. These observations are dealt with in more detail in the subsequent paragraphs.

It should be noted that in Figs. 5–10 that follow, the plotting of the results starts at 20 mm from the injector. The reason for this is that for most of the phenomena investigated the effects of system parameter variations are small over the first 20 mm from the injector. The expansion of the plots allowed by removing the first 20 mm ensures that the major variations further downstream are more discernible.

The temperature tests fall into a number of categories, with two temperatures that can be adjusted, namely the temperature at which the spray is injected and the initial temperature of the ambient gas. The effects on the droplet SMR obtained by adjusting the ambient temperature at low injection temperature are shown in Fig. 5(a). The SMR increases as the temperature is increased. This is the opposite effect to that seen in non-evaporating narrow cone sprays in which the number of collisions causes an increase in the droplet SMR as the density of the carrier gas increases. In this case, the gas density reduces with temperature but the SMR increases. This demonstrates that the effect is due to the heat up and evaporation of the liquid droplets. The smaller droplets evaporate more quickly than the large droplets. As a result the SMR increases due to the complete evaporation of small droplets and only larger droplets remaining. The vapour mass fraction along the centreline shown in Fig. 5(b) increases as the ambient temperature is increased as the gas exchanges more energy with the liquid heating the drops faster so that they evaporate more quickly. The exponential increase in the vapour mass fraction reflects the increase in the rate of mass exchange as the droplet temperature increases.

Very different behaviour is observed when the liquid is injected at the saturation temperature. The droplet sizes in these cases, as shown in Fig. 6(a), are much smaller due to even the large drops experiencing appreciable evaporation, and the sizes are much the same in each case. The rate of droplet size increase with axial distance also reduces in these cases as much of the liquid mass is evaporated so that there are fewer droplets and the rate of collisions reduces. The vapour mass fraction along the centreline in Fig. 6(b) is much greater in these cases due to the liquid evaporating at a fast rate immediately after injection. The reduction in the vapour mass fraction with axial distance is the result of two effects. Firstly, the spray is spread more in the radial direction at larger axial distances, so there is less liquid to evaporate around the centreline. Secondly, the rate of evaporation decreases due to the cooling of the surrounding gas as it loses heat to the droplets in order that they may evaporate. This cooling has more effect at lower ambient temperatures, and hence the vapour mass fraction is slightly higher when the ambient temperature is higher.

It should be noted that the conditions simulated in Fig. 6 would normally only apply in those cases where a

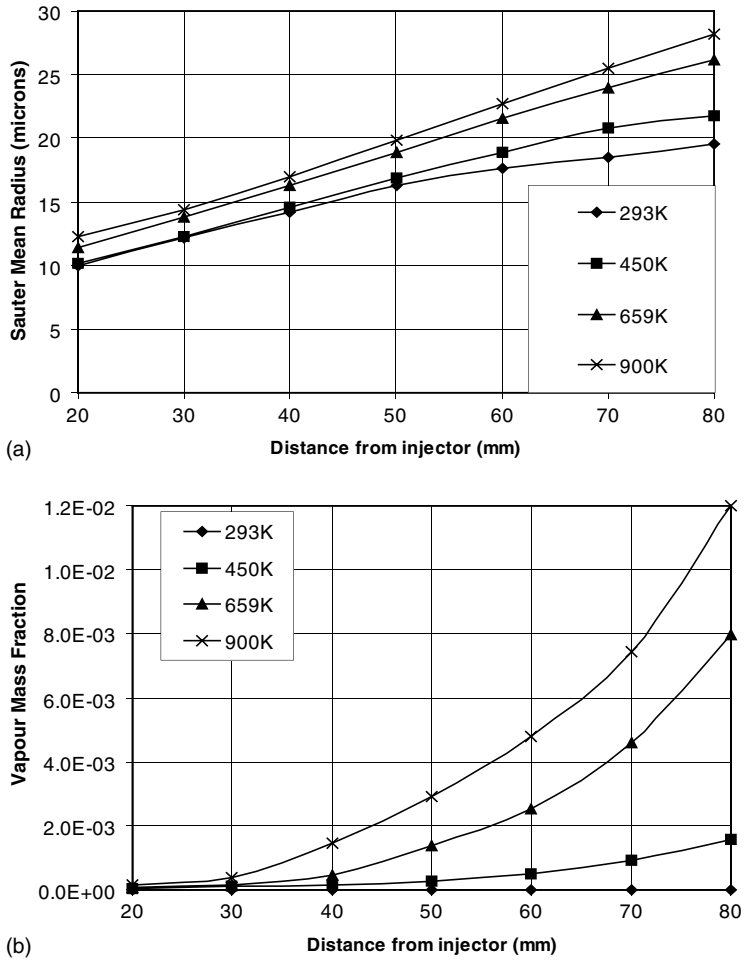

Fig. 5. Variations in (a) SMR and (b) centreline vapour mass fraction, with ambient gas temperature.

liquid is stored at or near its boiling temperature or in pressurised form at a temperature above its boiling temperature when released into the environment. However, it is important that the model be capable of predicting those sorts of conditions, as well as the conditions found in most fuel spray injections. For the conditions experienced here the form of the mass transfer number (Eq. (32)) should strictly be altered to include the fact that the surrounding vapour mass fraction will be significant in comparison with the value found at the drop surface, due to the large amounts of evaporation. Thus the proper equation to use would be

$$B_{\mathrm{M}} = \frac{f_{\mathrm{s}} - f_{\infty}}{1 - f_{\mathrm{s}}}, \tag{49}$$

where f_{∞} is the vapour mass fraction far from the drop. In reality for a finite-volume calculation procedure, as used here, this would be the value of f at the centre of the grid cell in which the drop resides. The results shown above will thus be an over-estimate of the mass evaporated, as use of Eq. (49) instead of Eq. (32) would reduce by a small amount the predicted amount of fuel evaporated.

Fig. 7 shows the effect of adjusting the injection temperature whilst maintaining the ambient gas temperature of 293 K. No evaporation takes place for the 293 K injection temperature case, and the droplet SMR increases downstream due to droplet collisions. The injection temperatures in the other two cases with higher temperatures are above the saturation temperature for the liquid, thus evaporation immediately takes place. The faster evaporation rate for the highest temperature case causes the droplet size to reduce, both directly due to the evaporation of the liquid mass and indirectly by the reduction of the number of collisions resulting from the existence of fewer droplets.

5.2. Evaporation models

The one-third rule (that is implemented in the model) is tested to find if it produces different results from other approximations for the droplet surface properties. The models are designated by the fraction of the gaseous temperature, x, used in the calculation of the droplet surface temperature. Hence

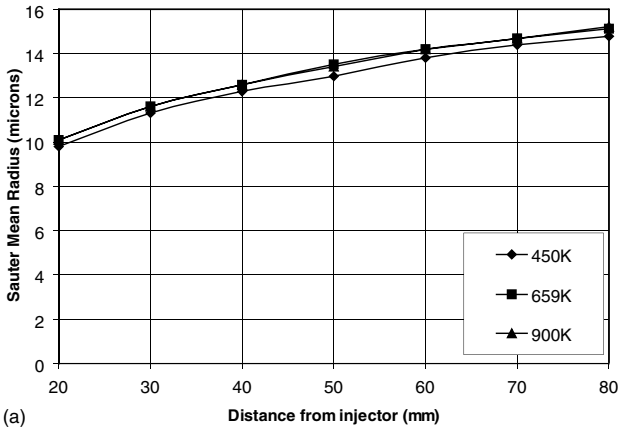

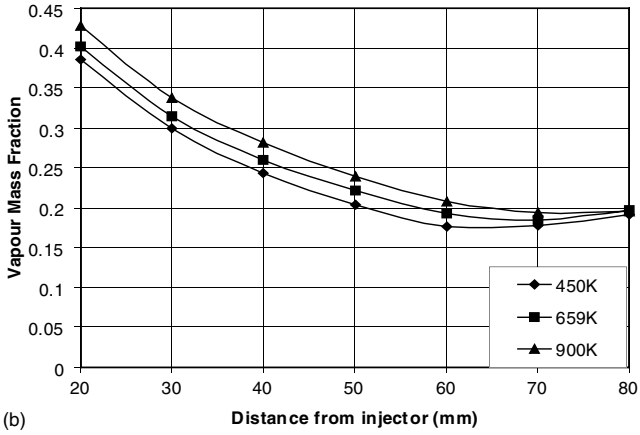

Fig. 6. Variations in (a) SMR and (b) centreline vapour mass fraction, with ambient temperature when the liquid is injected at saturation temperature.

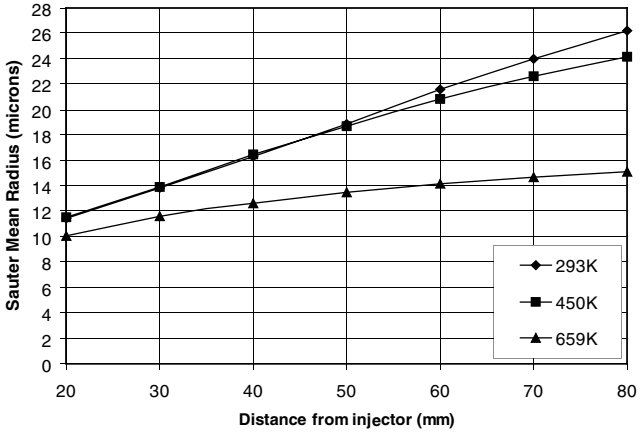

Fig. 7. Variation in SMR with injection temperature.

$$T_s = xT_g + (1-x)T_l. \tag{50}$$

The predicted drop sizes are almost independent of the value of x used; Beck (2000) shows a maximum variation of 3% by 80 mm downstream of the nozzle. Fig. 8 show that the vapour mass fraction in the base test case is also

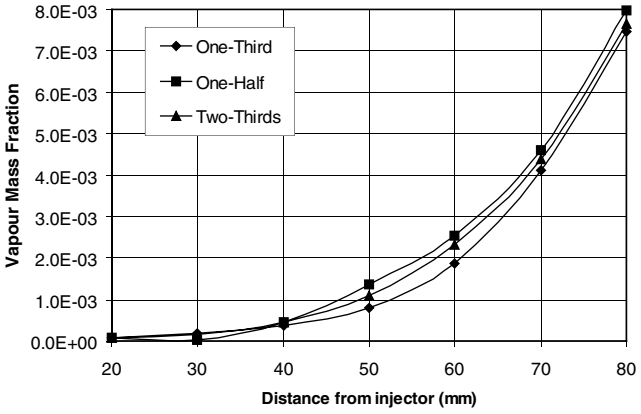

Fig. 8. Variation in vapour mass fraction with surface temperature model.

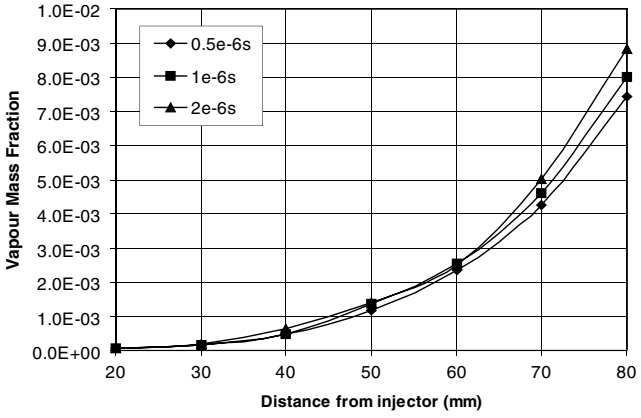

Fig. 9. Variation in centreline vapour mass fraction with computational time step.

relatively insensitive to the model used for the surface temperature. Thus, this case provides no evidence for one of the models to be used in preference to the others.

5.3. Numerical considerations

Over the range of time step used (0.5–2.0 μs) there are no appreciable effects on the droplet sizes produced, so this figure is not presented here. However, a small increase in the vapour mass fraction is seen in Fig. 9 as the time step is increased. The most likely explanation for this is that the heat transfer and evaporation are dependent on the liquid temperature at the beginning of the time step, and hence the temperature difference is maintained longer between the phases when a longer step size is used, resulting in a slightly larger increase in the droplet temperature in a given time. The effect is not large, of the order of 10% 80 mm downstream of the injector, so the results are reasonably independent of the time step.

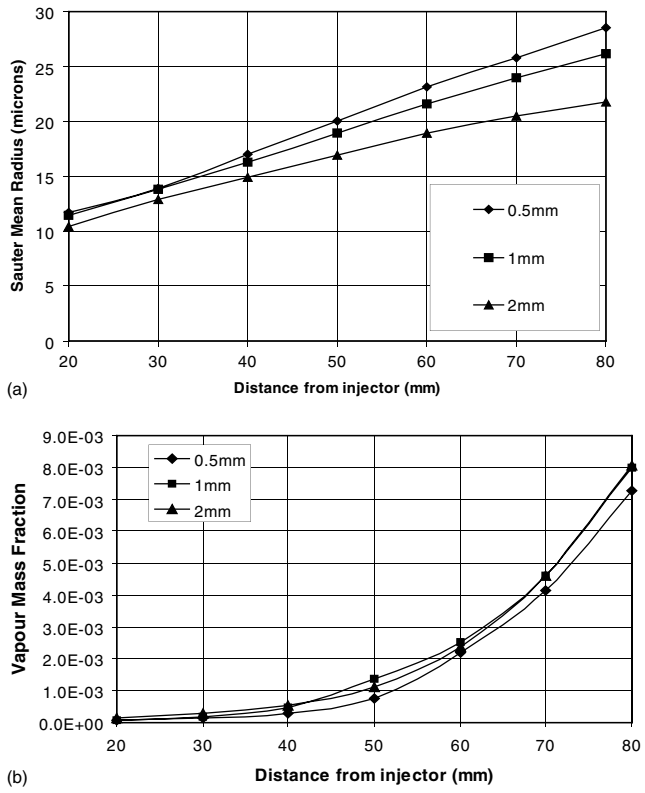

Fig. 10. Variations in (a) SMR and (b) centreline vapour mass fraction, with computational grid density, characterised by the longest side of the injection cell.

The fineness of the grid has a larger effect on the results, Fig. 10(a) showing that the predicted SMR is larger on a finer grid. This effect, which has also been noted for non-evaporating sprays (Beck, 2000) is due to the collisions model being more accurate with the use of a finer grid in the dense parts of the spray. The larger droplets evaporate less quickly, resulting in lower vapour mass fractions when the finest grid is used (Fig. 10(b)), although the difference is not great, being of the order of 10% 80 mm from the injector. The vapour mass fraction is no greater on the centreline using the coarsest grid than the second coarsest grid due to the enhanced numerical diffusion afforded by the coarseness of the grid. In order to run a finer grid than those already used, a smaller time step would be required, resulting in longer simulation times.

5.4. Comparison with experiment

5.4.1. Experiments of Solomon et al. (1985)

The first set of experiments used for validation are those of Solomon et al. (1985) in which freon-11 sprays are injected into air at approximately saturation pressure. Details are given in Table 2. The droplet sizes are measured using slide impaction and flash photography. Flash shadow photography was used for the combined measurements of drop size and velocity. Inlet and reference SMR values have been chosen to optimise the droplet size results. The injection domain has a maximum length of 1 mm. The grid used is very similar in structure to Fig. 4, having exactly the same number of grid lines in each direction, but it covers a larger area. This is 300 mm long by 100 mm wide in this case. The time step used was 5 μs. Predicted results are given after 0.5 s in both simulations, as the spray has been given ample time to reach approximately steady conditions. The results are plotted from 50 mm downstream of the injector because the first data collection point in both experiments was at or just beyond this point in the flow.

Table 2
Conditions for the experiments of Solomon et al. (1985)

	Case S1	Case S2
Injection velocity (ms^{-1})	64.5	29.64
Ambient pressure (kPa)	97	97
Spray angle	27°	29°
Nozzle radius (mm)	0.597	0.597
Injection temperature (K)	300	300
Ambient temperature (K)	300	300
Reference SMR (μm)	15	28
Inlet SMR (μm)	15	28

Fig. 11(a) presents the comparison of the experimental droplet SMR values on the axis of each spray with the values predicted by the model. The experimental results show approximately constant centreline SMR values in both cases. The model predicts lower values of SMR at an axial distance of 60 mm in Case S1, and also predicts that the SMR increases with distance, matching the experimental value on average, but not in detail. The low initial SMR values are most likely due to the model over-predicting the level of evaporation in the early stages of the spray. Initially the droplets become smaller, but eventually the smallest drops begin to disappear, and the SMR increases. The levels of evaporation in Case S2 are smaller due to the droplets being larger, and hence this phenomenon is not reproduced. In fact, the agreement between experiment and computation is very good in this case, even the slight increase in SMR with axial distance being successfully predicted. This is due to the low evaporation rate that causes a slight increase in the droplet SMR.

The comparison of the experimental and computational radial droplet SMR distributions at an axial distance of 60 mm is shown in Fig. 11(b). Apart from the small values of SMR at approximately 3 mm from the axis, for which there is no obvious explanation, the predicted SMR in Case S1 closely matches the experimental SMR, which is constant with radial distance. Presumably, high levels of evaporation in the 3 mm region cause the low SMR values there, and it is this locally high evaporation which results in the overall

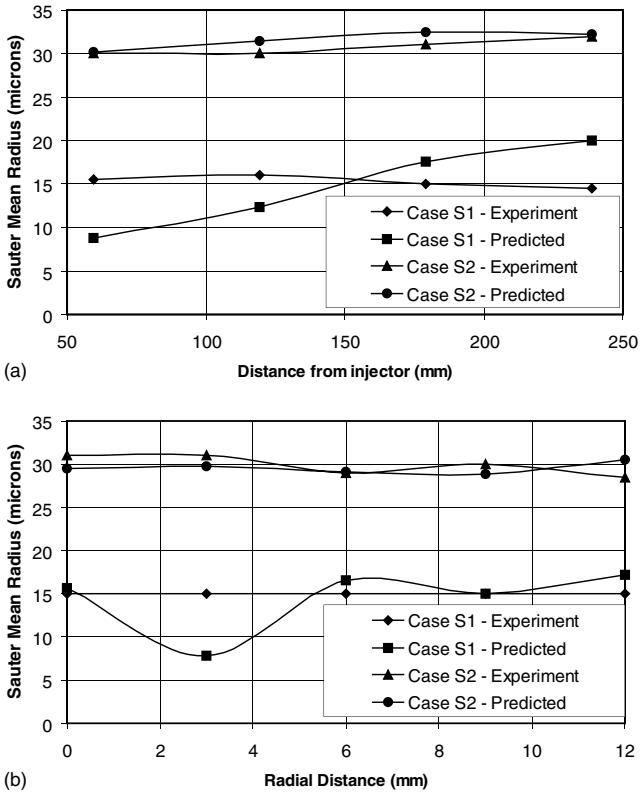

Fig. 11. Comparisons of (a) axial centreline SMR and (b) radial SMR distribution, with the experimental data of Solomon et al. (1985).

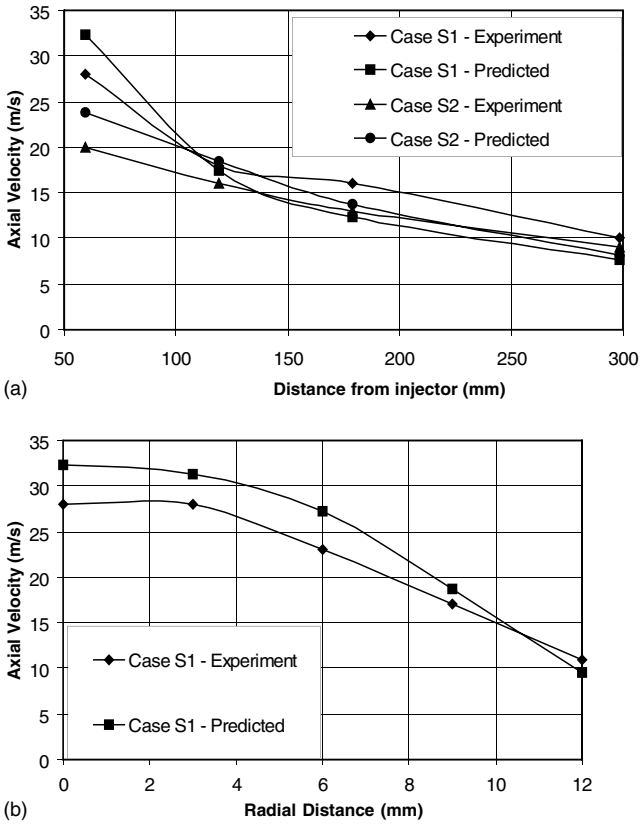

Fig. 12. Comparisons of (a) centreline axial droplet velocity and (b) radial distribution of axial droplet velocity, for case S1, with the experimental data of Solomon et al. (1985).

evaporation being slightly over-predicted. The Case S2 results show excellent agreement with the experimental droplet sizes. Again, the main difference between the cases is the larger droplets (and slower velocities) in Case S2, which result in lower evaporation levels. This suggests that it is the evaporation model causing the droplet SMR inaccuracies in Case S1, although which aspects of the model cause the problems is unknown.

In general, it is not appropriate to compare droplet velocity results obtained in experiment with the droplet velocities in the model. This is because the experimental results give a number-average velocity that is invariably lower than either the surface-area–average or mass–average velocities used in the model. The only exception is very near the centreline at significant axial distances from the nozzle where often all the droplets are found to have very similar velocities, as they are almost in equilibrium with the gas phase in this region. Hence, the experimental droplet velocities used for comparison in this case are for the larger droplets, as this best represents the mass–average velocity. The axial velocities found in experiment and computation are compared in Fig. 12(a). Case S1 shows a slight over-prediction of the velocity at 60 mm, but then a good rate of velocity decrease. This shows that the drag model is performing well, as has also been established for non-evaporating sprays in earlier publications. This also shows that the rate of evaporation cannot be too severely over-predicted, otherwise the velocity would reduce much more quickly with axial distance, due to the reduction in droplet momentum with the existence of much smaller droplets. The results for Case S2 are similar to those for Case S1 in that the velocity at 60 mm is slightly over-predicted, but then the rate of velocity decrease is again approximately correct.

Experimentally obtained radial distributions of axial droplet velocities are only given for Case S1 at 60 mm axial distance. The comparison of the experimental and computational values is presented in Fig. 12(b). Good agreement is seen between computation and experiment, with the slight over-prediction of droplet velocity seen in the centreline axial velocity values at 60 mm again being observed.

5.4.2. Experiment of Drallmeier and Peters (1994)

The second experiment used for validation of solid cone evaporating sprays is that of Drallmeier and Peters (1994) who injected an isooctane spray from a pressure swirl atomiser. Details of the experiment are given in Table 3. Droplet sizes and liquid volume fluxes were measured using phase Doppler anemometry and vapour concentrations were measured using an infrared extinc-

Table 3
Conditions for the experiment of Drallmeier and Peters (1994)

	Case D
Injection pressure (MPa)	0.415
Injection velocity (ms^{-1})	24.5
Ambient pressure (MPa)	0.1
Injection temperature (K)	323
Ambient temperature (K)	323
Spray angle	60°
Nozzle radius (mm)	0.23
Inlet mass flow rate (kg/s)	1.37×10^{-3}
Reference SMR (μm)	20
Inlet SMR (μm)	15

tion technique. The computational time step used was 4 μs and the injection cell had a largest side of 1 mm. The full grid employed is very similar to that used for the previous test cases, having the same number of grid lines in each direction and covering the same physical space.

The radial distribution of SMR produced by computation and experiment at three axial locations are compared in Fig. 13(a). The centreline values show good agreement at 50 mm from the injector, but at distances greater than 150 mm the computations predict larger values than given in the experiment. The experimental values increase with axial distance due to the evaporation of the smaller drops, and the results presented here suggest that the computations capture this effect as the computational values also increase. The increase in droplet size is, however, over-predicted which suggests that the preferential evaporation of the smaller droplets is too great in the computations. The rate of change of droplet size with radial distance is similar in computation and experiment, although the predicted values are of the order of 10 μm greater than the measured values. This is more evidence suggesting that the smaller droplets are evaporated more preferentially in the computation than in the experiment.

The comparison of the radial distributions of axial liquid mass flux at the same three axial locations is presented as Fig. 13(b). All three locations show that the spray is predicted as narrower by the computations than shown by the experiments. This is opposite to the error seen in wide-angle spray calculations (Beck (2000)). This suggests that the error is in the initial conditions, and that the uniform mass flux assumed at the downstream face of the injection cell(s) is inaccurate. In this case it appears that the mass is concentrated towards the larger radii, as would be seen in a hollow cone spray. Suggestions of error due to the first order nature of the discretisation scheme used also carry weight. The low liquid mass flux at the spray edge may also indicate that the computational model has a higher evaporation rate at larger radial distances than the experiments. This observation is supported by the vapour mass flux results, presented next.

Comparison of the radial distributions of axial vapour mass flux at the axial locations of 50, 150 and 250 mm is made in Fig. 13(c). Reasonable levels of agreement are seen between the experimental results and those predicted by the computation. At all three locations, the predicted vapour mass flux is slightly under-predicted at the centreline and slightly over-predicted at larger radial distances. This highlights the fact that the evaporation rate predicted is good, although slightly higher in general than that found in the experiments.

6. Conclusions

A new model has been developed for the simulation of poly-dispersed sprays. The model is based on evaluating the first four moments of the drop number distribution. To this end conservation and transport equations have been constructed for the third and fourth moments and their respective moment-averaged velocities. In addition, liquid energy and conservation equations for the gas phase are solved. The other moments of the number distribution are obtained by truncating an assumed number distribution. Sub-models relating to the hydrodynamics of the flow have been included here for completeness, but the main emphasis has been on the heat and mass transfer processes. The source terms in the liquid and gas phase conservation equations resulting from these processes have been derived.

In previous publications, Beck and Watkins (2002, 2003), of results obtained with the present model, the model has produced excellent spray penetration results in comparison with experimental data, thus validating the inter-phase momentum transfer model. The performance of the break-up and collisions models in dense narrow angle sprays has been validated by good predictions of droplet sizes. The model has been successfully applied to hollow cone sprays, producing good penetration and droplet size results. The collapse of the hollow cone was also evident in the predictions. The applications of the model have been less successful when simulating wide-angle full cone water sprays. It was concluded that this was due to incorrect assumptions concerning the inlet mass flow rate distributions.

In this paper the model has been applied to the simulation of evaporating sprays, both in a set of parametric tests and in comparison with experimental data. The parametric explorations have served to demonstrate that the model reacts in the correct qualitative manner to changes in input parameters. It has also been demonstrated that the model is not greatly affected by time step and grid dependence problems.

Overall, in comparison with experimental data, the evaporation model predicts good results, with a tendency to predict slightly high levels of evaporation. The distribution of vapour mass flux in Case D is well

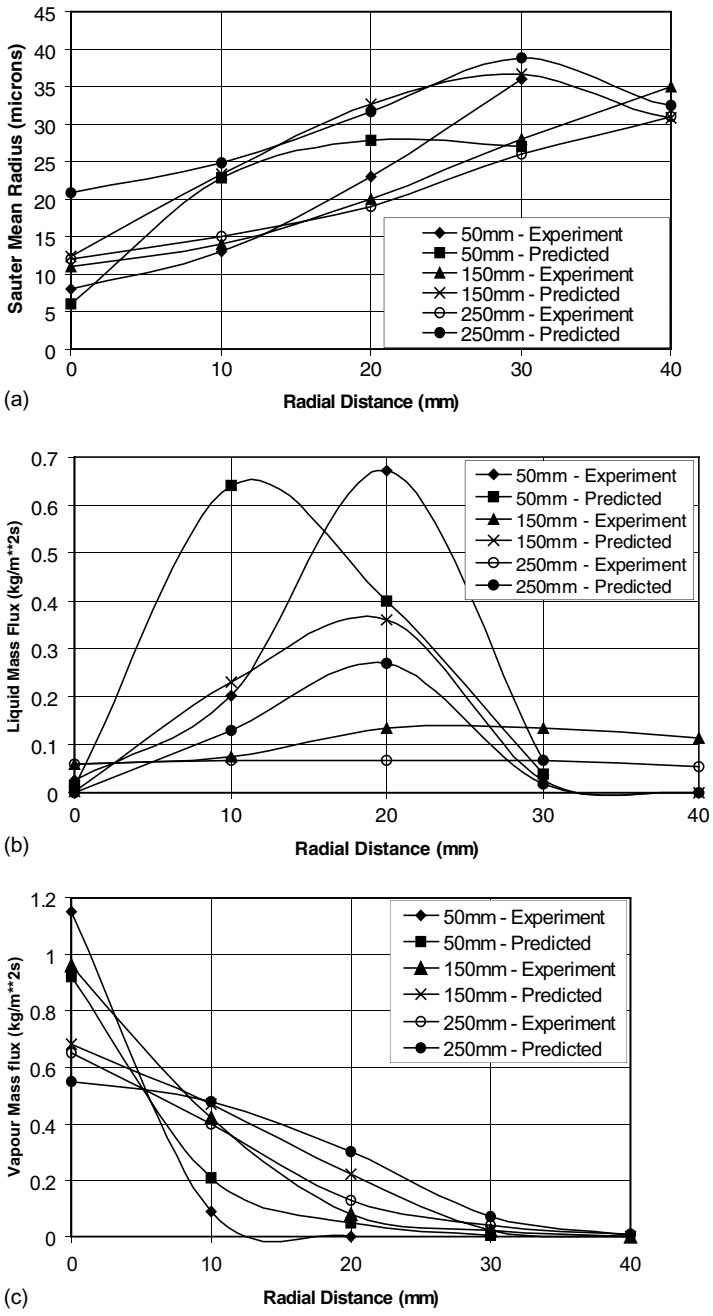

Fig. 13. Comparisons of radial distributions of (a) SMR, (b) liquid mass flux and (c) vapour mass flux, with the experimental data of Drallmeier and Peters (1994).

predicted. In test Case S2 where the droplet sizes are relatively large the predicted mean droplet sizes are in close agreement with experimental data, however in Case S1 the mean droplet sizes generally become too large as the preferential evaporation of small droplets is over-predicted.

Thus the model has been successfully applied to sprays involving heat transfer and evaporation, and the relevant sub-models have been assessed. A slightly more sophisticated evaporation model may be required in order to eliminate the effect of the smaller droplets evaporating too quickly in comparison with the larger droplets. The inadequacies of the present sub-model for evaporation in no way affect the basic correctness or otherwise of the moment-averaging approach to spray simulations.

There are a number of aspects of the heat and mass transfer sub-models that require further research, in the context of the moment-averaging approach. For example, as mentioned in Section 2.2, the model currently assumes that all drops locally have the same temperature, regardless of size, although the temperature can

vary in space and time. In reality, even on a local level, and certainly within the size scale defined by computational cells, the drop temperatures will vary, with the small drops heating up more quickly than large drops. A moment-averaging approach, similar to that used for moment-averaged velocity components, as outlined in Section 2.2, needs to be derived. This is the subject of on-going research.

References

Amsden, A.A., O'Rourke, P.J., Butler, T.D., 1989. KIVA-II: A computer program for chemically reactive flows with sprays. Technical Report LA-11560-MS, Los Alamos National Laboratory.

Beck, J.C., 2000. Computational modelling of poly-disperse sprays without segregation into droplet size classes. Ph.D. Thesis, UMIST.

Beck, J.C., Watkins, A.P., 2002. On the development of spray submodels based on droplet size moments. J. Comp. Phys. 182, 1–36.

Beck, J.C., Watkins, A.P., 2003. On the modelling of poly-disperse sprays without segregation into droplet size classes. Proc. R. Soc. Lond. A 459, in press. doi:10.1098/rspa.2002.1052.

Chen, X.Q., Perreira, J.C.F., 1992. Numerical predictions of evaporating and non-evaporating sprays under non-reactive conditions. Atomisation and Sprays 2, 427–433.

Crowe, C.T., 1982. Review—numerical methods for dilute gas-particle flows. Trans. ASME J. Fluids Eng. 104, 297–303.

Crowe, C.T., Sharma, M.P., Stock, D.E., 1977. The particle-source-in-cell (PSI-CELL) method for gas-droplet flows. Trans. ASME J. Fluids Eng. 99, 325–332.

Drallmeier, J.A., Peters, J.E., 1994. Liquid and vapour phase dynamics of a solid cone pressure swirl atomiser. Atomisation Sprays 4, 135–158.

Ducowicz, J.K., 1980. A particle-fluid numerical model for liquid sprays. J. Comp. Phys. 35.

Gosman, A.D., Johns, R.J.R., 1980. Computer analysis of fuel-air mixing in direct injection engines. SAE Paper 800091.

Harlow, F.H., Amsden, A.A., 1975. Numerical calculation of multiphase fluid flow. J. Comp. Phys. 17, 19–52.

Jiang, Y.J., Umemura, A., Law, C.K., 1992. An experimental investigation on the collision behaviour of hydrocarbon droplets. J. Fluid Mech. 234, 171.

Levy, N., Amara, S., Champoussin, J.C., Guerrasi, N., 1997. Non-reactive diesel spray computations supported by PDA measurements. SAE Paper 970049.

Liu, A.B., Reitz, R.D., 1993. Mechanisms of air assisted atomisation. Atomisation Sprays 3, 55.

Melville, W.K., Bray, K.N.C., 1979. A model of the two-phase turbulent jet. Int. J. Heat Mass Transfer 22, 647–656.

Mostafa, A.A., Elghobashi, S.E., 1985. A two-equation turbulence model for jet flows laden with vaporizing droplets. Int. J. Multiphase Flow 11, 515.

Mostafa, A.A., Mongia, H.C., 1987. On the modelling of turbulent evaporating sprays: Eulerian versus Lagrangian approach. Int. J. Heat Mass Transfer 30, 2583.

Orme, M., 1997. Experiments on droplet collisions, bounce, coalescence and disruption. Prog. Energy Comb. Sci. 23, 65.

O'Rourke, P.J., Bracco, F.V., 1980. Modelling of drop interactions in thick sprays and comparison with experiment. Stratified Charge Auto Engines Conf. IMechE, London.

Ranz, W.E., 1958. Some experiments on orifice sprays. Can. J. Chem. Eng. 36, 175.

Ranz, W.E., Marshall, W.P., 1952. Evaporation from drops. Chem. Eng. Prog. Part 1 48, 141–146.

Reitz, R.D., 1987. Modelling atomisation processes in high-pressure vaporising sprays. Atomisation Spray Tech. 3, 309.

Solomon, A.S.P., Shuen, J.S., Zhang, Q.F., Faeth, G.M., 1985. Measurements and predictions of the structure of evaporating sprays. Trans. ASME J. Heat Transfer 107, 679–686.

Spalding, D.B., 1953. The combustion of liquid fuels, 4th Int. Symp. Comb.

Wang, X.F., Lefebvre, A.H., 1987. Influence of ambient air pressure on pressure-swirl atomisation. Atomisation Spray Tech. 3, 209.

Watkins, A.P., 1989. Three-dimensional modelling of gas flow and sprays in diesel engines. In: Markatos, N.C. (Ed.), Computer simulation for fluid-flow, heat and mass transfer and combustion in reciprocating engines. Hemisphere.